Supplementary

DEVELOPMENT OF A PCB- BASED ELECTROCHEMICAL APTASENSOR FOR CHIKUNGUNYA VIRUS PROTEIN DETECTION

Syama Sajikumar ‡[a], Naveenkumar Sureshkumar ‡[a,b], VVR Sai [b], Verma Jyoti [c], Sujatha Sunil [c], Ramanathan Srinivasan [a]

Affiliation

[a] Department of Chemical Engineering, Indian Institute of Technology Madras, Chennai 600036, India

[b] Department of Applied Mechanics and Biomedical Engineering, Indian Institute of Technology Madras, Chennai 600036, India

[c] Vector-borne diseases, International Centre for Genetic Engineering and Biotechnology, New Delhi 110 067, India

S1. CHIKV E1 protein

Expression and purification of CHIKV E1 protein

Recombinant CHIKV E1 protein was expressed in Escherichia coli BL21 (DE3) CodonPlus cells transformed with the pET-29a-E1 construct, as described previously (Kumar et al., 2022) with modifications. Briefly, cultures were grown in Terrific Broth containing 25 μg/mL kanamycin at 37 °C with shaking at 180 rpm. When the optical density at 600 nm (OD_{600}) reached 0.6–0.8, protein expression was induced by adding 1 mM isopropyl-β-D-thiogalactopyranoside (IPTG), followed by incubation at 18 °C for 16 h. Cells were harvested by centrifugation and expression of the E1 protein was confirmed by 12% SDS-PAGE and Coomassie brilliant blue staining.

For purification, the bacterial pellet was resuspended in lysis buffer (50 mM Tris-Cl, pH 8.0; 150 mM NaCl; 5% glycerol; 2 mM β-mercaptoethanol; 1 mM PMSF; and lysozyme), lysed by sonication, and centrifuged at 11,000 rpm for 30 min at 4 °C. The insoluble fraction was solubilized in lysis buffer containing 8 M urea and incubated at 37 °C for 2 h with shaking. The clarified lysate was incubated with Ni-NTA agarose beads (1 mL) overnight at 4 °C. The column was washed with lysis buffer containing 8 M urea and increasing concentrations of imidazole (30 mM and 50 mM), and the bound protein was eluted using buffer with 100–500 mM imidazole. Eluted fractions were analyzed by SDS-PAGE and stored at –80 °C. Urea was removed by stepwise dialysis against 50 mM Tris-Cl (pH 8.0) containing 300 mM NaCl.

SDS-PAGE AND WESTERN BLOTTING.

E1 purified protein was first resolved on 12% SDS-PAGE along with a protein marker and transferred to a nitrocellulose membrane (Bio-Rad, Hercules, CA, USA, Cat No. 1620112) for 1h at 60V in ice cold transfer buffer (25 mM Tris, 192 mM glycine, pH 8.3, 0.1% SDS and 20% methanol). The membrane was then blocked using 5% BSA in PBS for 1 hr at room temperature. Subsequently, the membrane was washed three times with 1X PBST. Next, the membrane was incubated with the lab-generated anti-E1 polyclonal antibody (Kumar *et al.*, 2023) at 1:5000 dilution overnight. After washing three times with PBST for 10 min, the membrane was incubated for 1 hr at room temperature with HRP-conjugated sheep anti-mice IgG (Novus Biologicals, Cat. NB7539, Centennial, CO, USA) at 1:10000 dilution. After washing three times with PBST, the membrane was visualized using SuperSignal® West Pico Chemiluminescent Substrate (Thermo Fisher Scientific Inc., Waltham, MA, USA) in the Bio-Rad ChemiDoc MP system (Hercules, CA, USA).

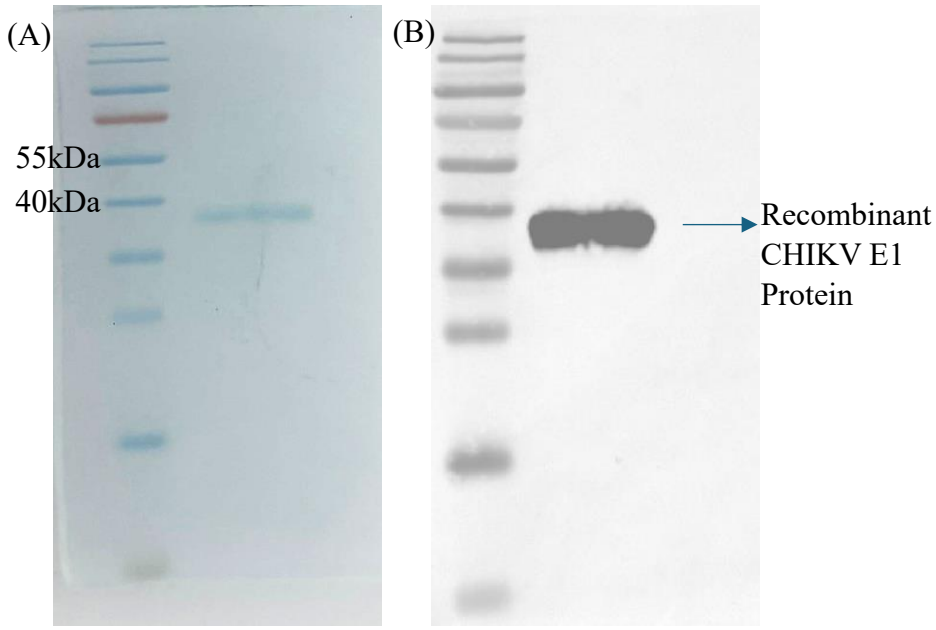

Figure S1.1 The affinity chromatography purified recombinant CHIKV E1 protein was resolved on 12 % SDS PAGE and stained with **A)** Coomassie brilliant blue as well as same was **B)** immunoblotted with anti-CHIKV E1 antibody and showed band at size range of 37 kDa.

Gel Permeation Chromatography of Recombinant E1 Protein

The recombinant CHIKV E1 protein was initially purified using Ni–NTA affinity chromatography, and its purity was verified by 12% SDS–PAGE. The purified eluted protein was then concentrated to a final concentration of 1.2 mg/mL and subjected to gel permeation chromatography (GPC) to evaluate its biophysical quality. For size-exclusion separation, a Superdex 75 column was pre-equilibrated with GPC buffer containing 50 mM Tris-HCl, 150 mM NaCl, and 5% glycerol. . A total of 2 mL of concentrated E1 protein sample was loaded onto the injection loop, and protein elution was performed at a flow rate of 0.5 mL/min. The resulting chromatogram displayed a single symmetric peak, suggesting a monodisperse and homogeneous protein population. Fractions corresponding to the major peak (C4-D12) were collected and analyzed by 12% SDS-PAGE. Coomassie Brilliant Blue staining revealed a prominent band at ~37 kDa, consistent with the expected molecular weight of E1, confirming the purity and structural integrity of the protein in the peak fractions.

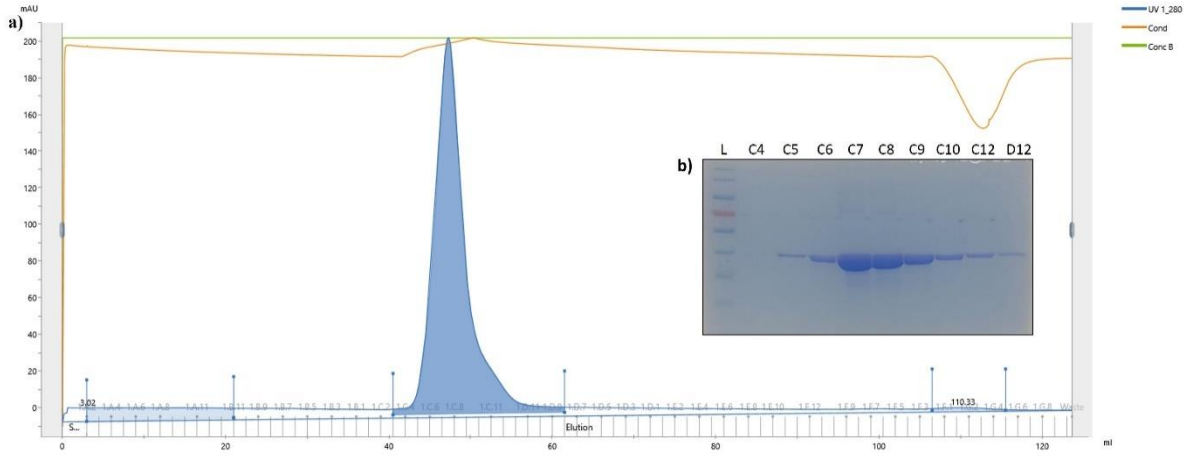

Figure S1.2 Gel permeation chromatography (GPC) profile of recombinant CHIKV E1 protein with SDS-PAGE analysis of eluted fractions

(a) The recombinant CHIKV E1 protein (4.2 mg total protein) was subjected to gel permeation chromatography. The GPC chromatogram exhibited a single symmetrical peak, indicating a homogeneous protein population. Fractions corresponding to the major peak (C4–D12) were collected for analysis.
(b) Peak fractions were resolved on a 12% SDS-PAGE gel and stained with Coomassie Brilliant Blue. A distinct band at ~37 kDa was consistently observed across these fractions, confirming the presence, purity, and integrity of the E1 protein within the eluted peak.

S2. Aptamer preparation

Resuspension and folding buffers were provided by the aptamer vendor (Base Pair Technologies, TX, USA). First, the aptamer was dispersed in the resuspension buffer to achieve a concentration of 100 μM. To form the proper tertiary structure, the aptamer suspension was diluted with the folding buffer to 10x–100x the final concentration and heated to 90–95 °C for 5 minutes. The mixture was subsequently cooled to room temperature under natural convection (10–15 minutes). Next, the solution was mixed with an equal volume of 20 mM Tris(2–carboxyethyl) phosphine (TCEP) reducing buffer for 90 min to break the disulfide bonds. TCEP is known to break the disulfide bonds[1-3]. This step is essential for the immobilization of the aptamer on the gold electrode via the thiol group. Finally, the solution was diluted with 10 mM PBS containing 1 mM $MgCl_2$ to the desired aptamer concentration.

S3. Photographs of the special connector used to attach the PCB sensor to a potentiostat

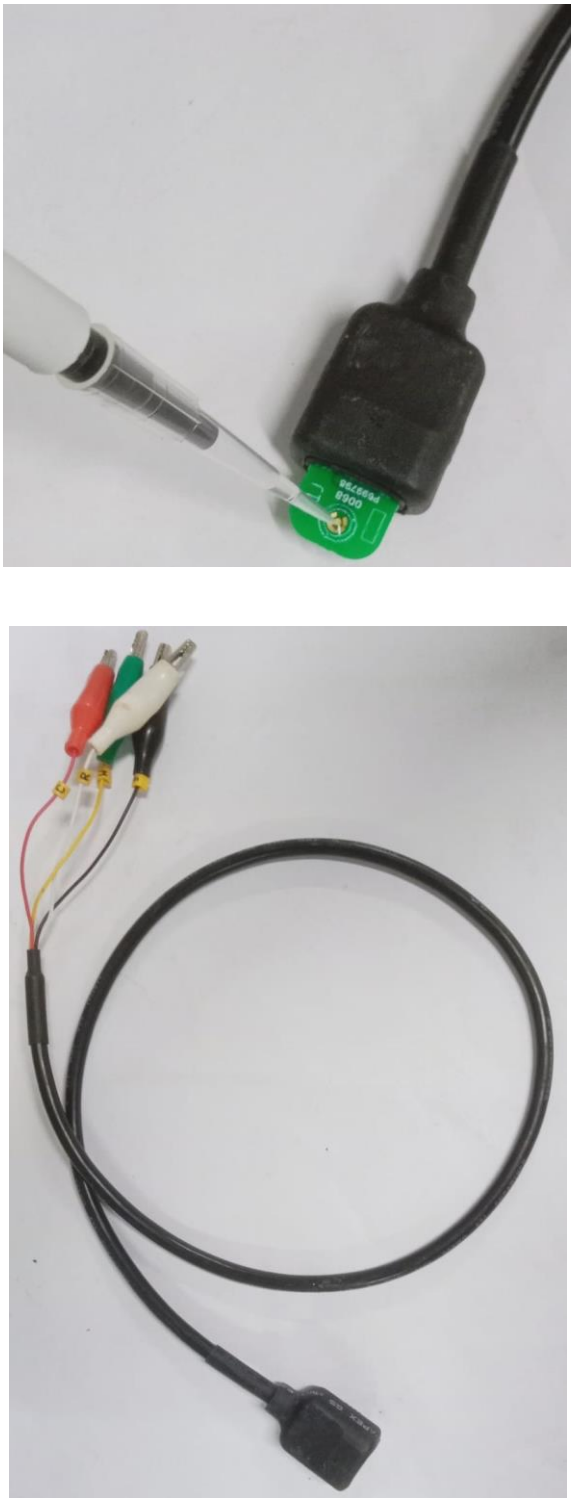

Figure S3 Photographs of the PCB connector

S4. PCB electrode cleaning trials

Literature describes several methods to clean Au surface [4, 5] and a few are evaluated in this study. In one case, a 20 µL drop of isopropyl alcohol (IPA) was placed on the sensor for 5 min. In alcohol sonication, a mix of 50% ethanol and 50% methanol was used and the sensor was immersed in the alcohol mixture and sonicated for 5 minutes. In the third case, a 20 µL drop of 50 mM sulfuric acid was placed on the sensor 5 min. In the fourth cleaning method, 20 µL of a mix of 50 mM KOH and 30 % H_2O_2 (2:1 volume ratio) was placed on the sensor for 5 min. All the above experiments were conducted at room temperature (~ 27 °C). In the fifth case, the sensor was immersed in a mix of 25 % NH_4OH and 30% H_2O_2 (in 2:1 volume ratio) at 40 °C for 3 min. In all the cases, after the cleaning process, the sensor was rinsed in MilliQ® water and dried in an N_2 stream.

The electrode was subjected to SEM analysis both before and after cleaning. The SEM images of the electrode before and after each cleaning process are shown in Fig. S4.1. The initial surface (Fig. S4.1a) was rough, and cleaning with dilute H_2SO_4 (Fig S4.1d) reduced the roughness. The other cleaning processes do not appear to reduce the roughness significantly.

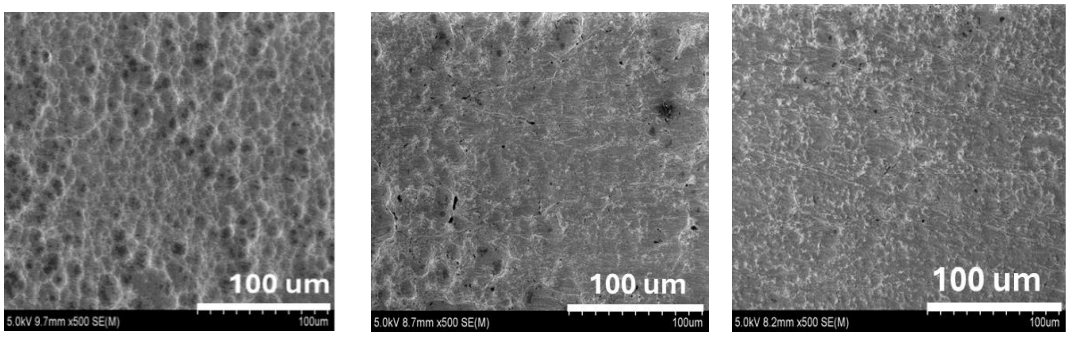

(a) (b) (c)

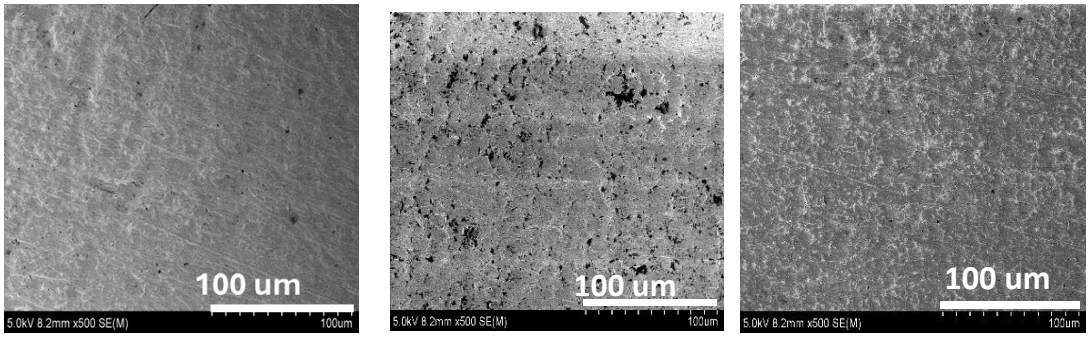

(d) (e) (f)

Figure S4.1 SEM image of the PCB electrode before and after cleaning. a) Fresh Electrode, b) IPA, c) Alcohol sonication, d) dil. H_2SO_4 e) KOH-H_2O_2 and f) NH_4OH-H_2O_2

Cyclic voltammogram studies were performed with the sensors and the results (Fig. S4.2) show that all of them exhibit a good response. A slightly higher peak response observed in the sensors leaned using NH_4OH - H_2O_2 mixture.

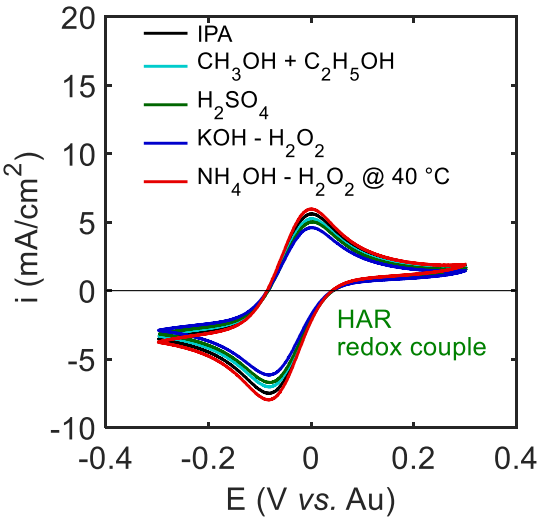

Figure S4.2 CV of the electrode after treated with different chemicals

After the electrodes were treated with aptamer, MCH and CHIKV E1 protein during sensing, the sensors were cleaned again using these five protocols, and signal recovery was good and repeatable when NH_4OH - H_2O_2 mixture was used (results not shown). Therefore, NH_4OH - H_2O_2 mixture cleaning was employed in all the subsequent experiments.

S5. Dimensionless kinetic parameter measurements

Cyclic voltammograms of the fresh electrode was acquired at several potential scan rates, from 20 mV/s to 2 V/s. The cathodic (i_{pc}) and anodic (i_{pa}) peak current densities were recorded. The separation of peak potential (ΔE_p) was also recorded.

Using the Randles Sevcik equation, we get

$$i_p = 0.446nFAC\sqrt{\frac{nFD\nu}{RT}} \quad i_p = 0.446\frac{F^{3/2}}{\sqrt{RT}}AD^{1/2}n^{3/2}\nu^{1/2}C = 2.69\times10^5 AD^{1/2}n^{3/2}\nu^{1/2}C$$

Therefore, $A = \frac{1}{2.69\times10^5 \times D^{1/2}n^{3/2}C} \times \frac{i_p}{\nu^{1/2}}$

Based on this formula, with n=1, C = 25 mM, diffusivity[6] of Ru(III) = 7.7 × 10^{-6} cm^2/s, the electrochemically active area is found to be 2 times larger than the geometric area. i.e., Roughness factor = 2.

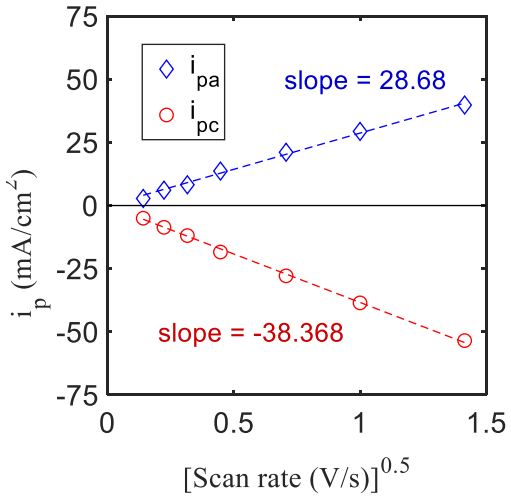

Figure S5 CV peak current value *vs.* square root of the scan rate

The dimensionless kinetic parameter ψ was calculated using the formula [6]

$$\psi = \frac{-0.6288 + 2.1\Delta E_p}{1 - 17\Delta E_p}$$

The ΔE_p varied between 81 to 161 mV, and the ψ value varied between 1.22 to 0.17.

$$\psi = \frac{k_0}{\left(\frac{n\pi D_0 F \nu}{RT}\right)^{0.5}} = \frac{k_0}{\left(\frac{n\pi D_0 F}{RT}\right)^{0.5}} \frac{1}{(\nu)^{0.5}}$$

Using the above formula, the rate constant k_0 is estimated to be 0.006 cm/s.

S6. Summary of EDX analysis of PCB

The EDX results of fresh PCB surface, after experiments in HAR and after experiments in Ferro/Ferri redox couple were analysed to calculate the weight % of the major constituent elements. The results, presented in Fig. S6, show that when the sensor was evaluated using Ferro/Ferri redox couple, the Au content decreased and Ni and Cu content increased, indicating that the Au was attacked by Fe^{2+}/Fe^{3+} redox couple. On the other hand, when the sensor was evaluated in HAR redox couple, there is very little change in the weight % of the elements, confirming that the HAR redox couple does not attack the Au surface.

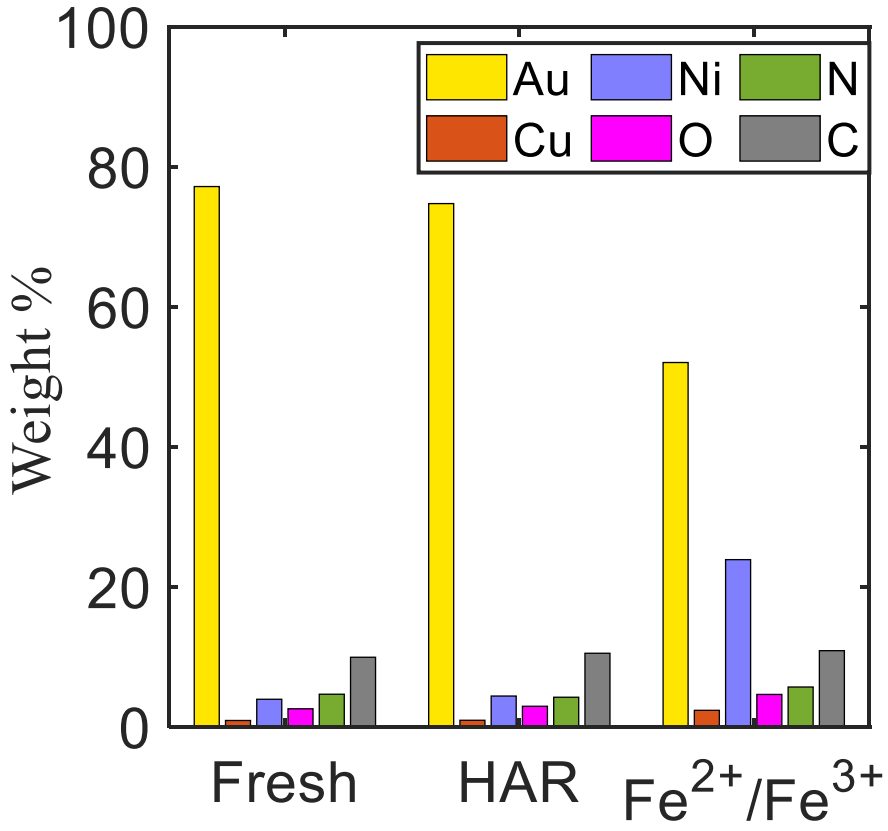

Figure S6 A comparison of the wt % of elements on the electrode surface, measured by EDX, for fresh electrode, after exposure to HAR and after exposure to ferro/ferri redox couple

S7. Signal repeatability within and across PCB electrodes

The SWV signals in HAR and Fe^{2+}/Fe^{3+} redox couple are presented below. Each PCB sensor was tested 5 times, and five different sensors were employed for each solution. A comparison of the signal response within and across different PCB electrodes confirms that HAR redox couple yield better signal repeatability than $K_4[Fe(CN)_6]$ / $K_3[Fe(CN)_6]$ redox couple.

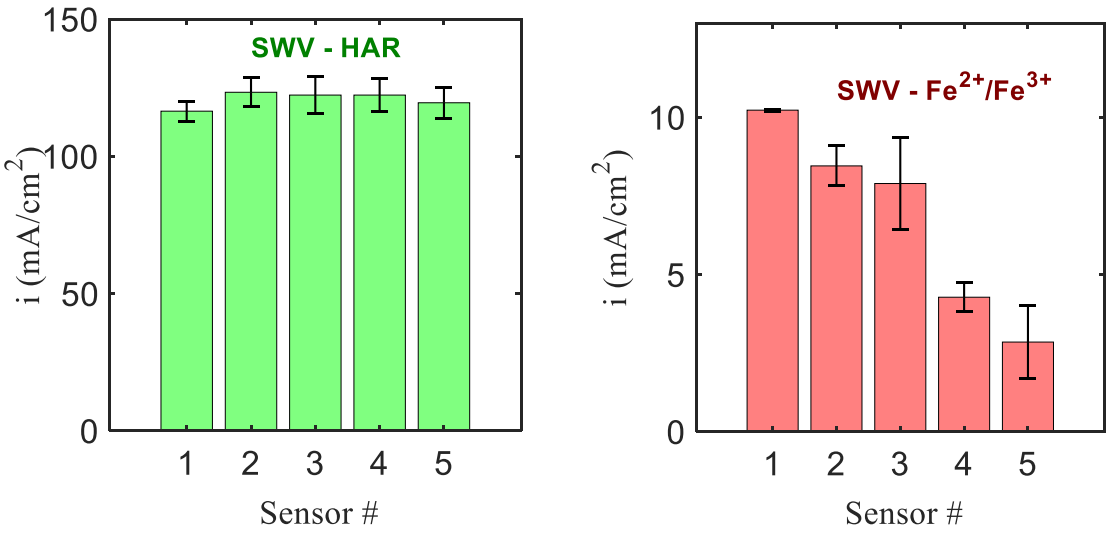

Figure S7 SWV peak values in (a) HAR and (b) ferro/ferri redox couple. The error bars represent the variations in multiple measurements on the same electrode.

S8. Estimation of aptamer surface coverage on PCB electrode

The surface coverage has also been estimated using EIS in literature. In one method, a formula relating the charge transfer resistance (R_{ct}) to surface coverage can be used[7]. This formula of surface coverage estimate is appropriate when electrochemical impedance spectroscopy (EIS) data are analysed. The R_{ct} value cannot be estimated from SWV measurements. Although EIS is a versatile technique often used in biosensing, we have employed SWV due to the quicker measurement time, and simpler electronics required (which will be important for future miniaturization of the measurement device).

Based on a similar logic to the above formula, SWV peak measurement can be taken as an indicator of surface coverage and we can estimate $\theta = \left(1 - \frac{i_{p-apt}}{i_{p-fresh}}\right) \times 100\%$. For 200 nM aptamer (without MCH), the peak current value decreased from 123 mA/cm^2 (fresh electrode) to 99 mA/cm^2 (with Aptamer). This corresponds to a surface coverage of 0.195, or 19.5%. However, this method of using SWV results has not been used in literature. A detailed comparison between the surface coverage values estimated using SWV and EIS is beyond the scope of this work.

S9. Optimization of aptamer and CHIKV E1 incubation time

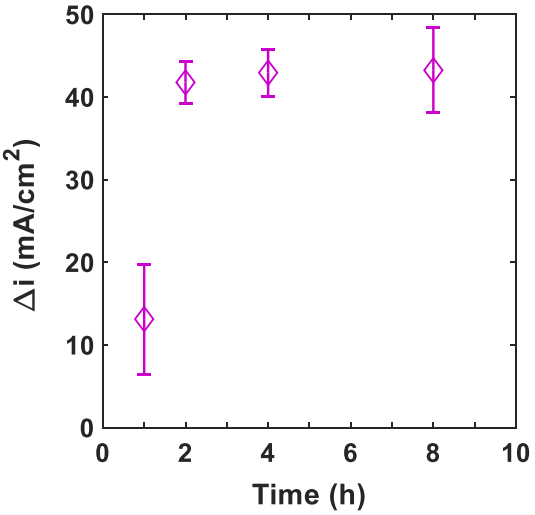

Figure S9.1 Change in SWV peak current due to 200 nM Aptamer + 10 μM MCH binding on Au surface, as a function of time. There is no significant change in the average signal after 2 h.

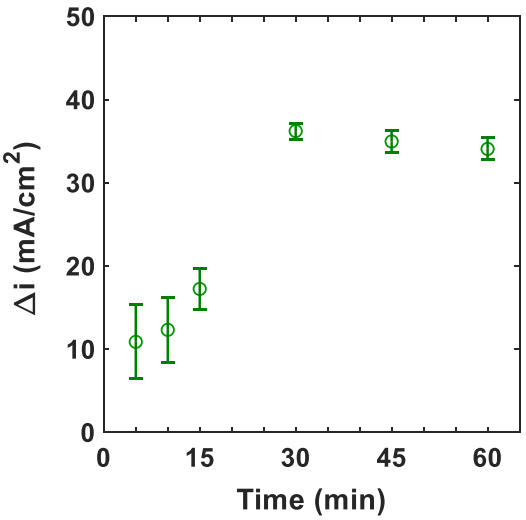

Figure S9.2 Change in SWV peak current due to binding of 100 nM CHIKV E1 protein on aptasensor (200 nM Aptamer + 10 μM MCH on Au) surface, as a function of time. There is no significant change in the average signal after 30 min.

S10. Aptamer and CHIKV E1 protein interactions

The interaction parameters B_{max}, and K_D can be estimated by relating the electrochemical measurements to the surface coverage. If the interaction between the target analyte and the immobilized aptamer can be modelled using Langmuir adsorption isotherm, then these parameters can be extracted. For example, based on charge transfer resistance (R_{ct}) values obtained using electrochemical impedance spectroscopy (EIS), literature report[7] has estimated B_{max}, and K_D.

EIS is a very sensitive technique, and it requires more time and more sophisticated electronics compared to SWV. On the other hand, SWV requires a very short time and less sophisticated electronics, which makes it more amenable to miniaturization. In the literature employing EIS, the trend of change in R_{ct} (ΔR_{ct}) was related to the concentration, to obtain B_{max} in Ω and K_D in nM.

$$\Delta R_{ct} = \frac{B_{\max}\left[\text{Target}\right]}{K_D + \left[\text{Target}\right]}$$

In this study, we employ SWV, and the trend of change in current density (Δi) with concentration can be related to the concentration, to obtain B_{max} in mA/cm^2 and K_D in nM.

$$\Delta i = \frac{B_{\max}\left[\text{CHIKV E1 concentration}\right]}{K_D + \left[\text{CHIKV E1 concentration}\right]}$$

This can be written as $\frac{1}{\Delta i} = \frac{1}{B_{\max}} + \frac{K_D}{B_{\max}} \frac{1}{\left[\text{CHIKV E1 concentration}\right]}$.

Our results indicate that except at very high and very low concentrations of CHIKV E1, the interaction between the CHIKV E1 and the aptamer is described by Temkin isotherm model. i.e., Δi is related to the log of the CHIKV E1 concentration. However, at very high concentrations, the Δi values saturate, indicating that Langmuir model is applicable. Using the results at high concentrations, the parameters B_{max} and K_D are obtained.

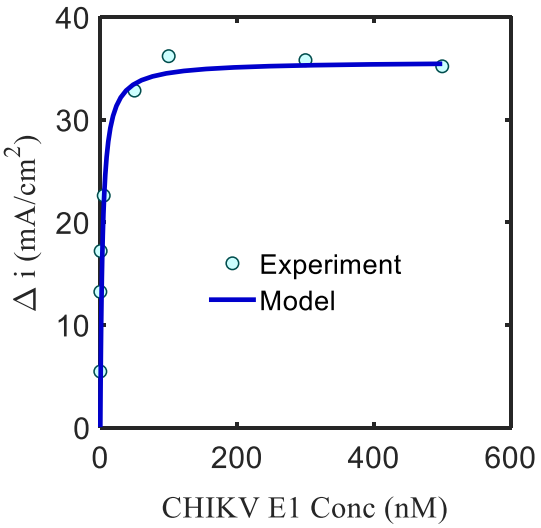

Figure S10 Change in SWV signal vs. CHIKV E1 concentration.

The model parameters are B_{max} = 35.7 mA/cm^2 and K_D = 3.26 nM.

S11. Intra- and inter-batch variations

In order to assess the intra-batch and inter-batch variations, multiple samples of 10 nM CHIKV E1 were evaluated on different days. The results show that the relative standard deviations (RSD) of intra-batch and inter-batch variations are < 10%.

Intra-batch variations

Batch No.	Signal Average (mA/cm^2)	Signal Standard deviation (mA/cm^2)	RSD
1	27.7	1.15	4.15%
2	27.0	1.08	4.02%
3	26.7	1.13	4.24%
4	26.9	1.67	6.22%

Inter-batch variation.

Mean value = 27.1 (mA/cm^2),

Standard deviation = 0.43 (mA/cm^2),

RSD = 1.58%

S12. Modified LOD formula

Usually, the LOD is calculated using the formula $\text{LOD} = \frac{3.3\times \text{ stdev}}{\text{slope}}$, where the *slope* refers to the ratio of the signal to the concentration in the linear range, and *stdev* refers to the standard deviation in the signal. This formula is valid when the signal is directly proportional to the analyte concentration. When the signal is linearly related to the logarithm of the analyte concentration, this has to be modified, as illustrated below.

The concentration can be expressed in several different units. In this example, we have expressed concentration in three different units, viz. fM, pM and nM. The calibration curves of signal vs. $\log_{10}$(Concentration), with only the data points in the linear part, are shown for simplicity.

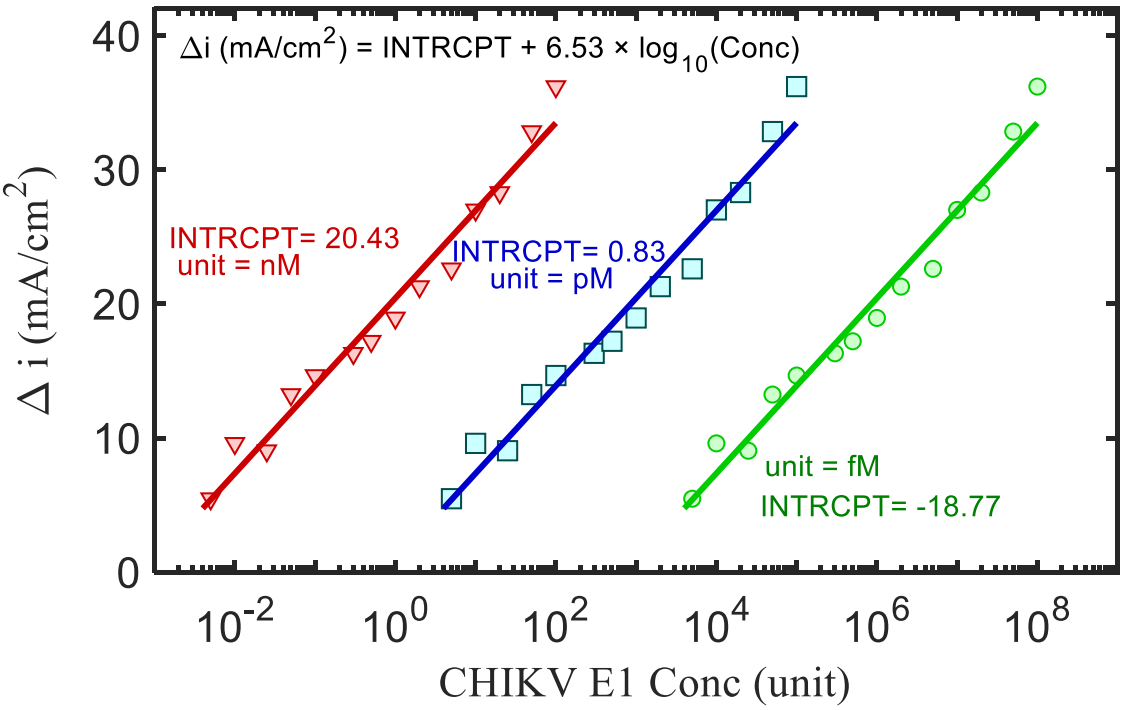

Figure S12 Calibration curve showing Δi *vs.* $\log_{10}$(CHIKV E1 concentration) in three different concentration units.

Please note that the slope is the same in all the three cases, while the intercept values are different. i.e., changing the concentration unit does not change the slope, but changes the intercept.

The LOD is defined as the concentration corresponding to the smallest signal that can be distinguished from a blank sample with certain level of confidence (3.3 × stdev). Here, blank

has a concentration of zero analyte, and log10(0) is -∞, which cannot be shown in the plot. This issue affects all calibration curves where the signal is linearly related to the *logarithm* of the analyte concentration. This issue does not arise when the signal is linearly related to the analyte concentration.

Here, if we directly use the traditional 3σ formula that $\text{LOD}=\frac{3.3 \times \text{stdev}}{\text{slope}}$, with stdev = 2.2 mA/cm^2, and slope = 6.53 $\text{mA/cm}^2/\log_{10}(\text{Conc(units)})$, we get a result that

LOD =1.11 in $\log_{10}(\text{Conc(units)})$,

which corresponds to 12.88 (~ 13) units, regardless of the units.

In other words, based on whether the units chosen are fM, pM or nM, the LOD is estimated as 13 fM, or 13 pM or 13 nM. Obviously, the standard formula is not appropriate when the signal is linearly related to the logarithm of the analyte concentration.

In this case, we may assume that the signal is zero at and below a certain analyte concentration, called $C_{\text{zero-signal}}$. Then we can define LOD as the concentration corresponding to the smallest signal that can be reliably distinguished from $C_{\text{zero-signal}}$.

For each case, we can estimate $C_{\text{zero-signal}}$, as per the calibration formula. This is given by

Signal = intercept + slope × $\log_{10}(C_{\text{zero-signal}})$= 0,

i.e., $\log_{10}(C_{\text{zero-signal}})$ = -intercept/slope.

Now, LOD can be estimated using the modified formula $\text{LOD}=\frac{3.3 \times \text{stdev - intercept}}{\text{slope}}$

Using the modified formula, we get LOD = -2.01 in $\log_{10}(\text{Conc(nM)})$, 0.9846 in $\log_{10}(\text{Conc(pM)})$, and 3.99 in $\log_{10}(\text{Conc(fM)})$, all of which correspond to the same LOD value of ~10 pM.

We note that if the slope value is much larger than the intercept value (i.e., -intercept/slope is very small compared to 3.3 × stdev/slope), the correction to the standard formula will be small. Then the LOD estimated by the standard formula will be close to the correct LOD.

We reiterate that this issue does not arise when the signal is directly proportional to the concentration and the intercept is zero. In that case, when different units are used, the signal vs. concentration slope value will change and all the LOD estimates will be identical.

S13: Calculation of confidence intervals of calibration curve parameters

Fourteen points were used in the calibration curve (Fig. 7c). The standard errors, t-test and p-test values, and the 95% confidence interval values were calculated using Microsoft Excel® Data Analysis tool and the results are shown below.

Table S13. Calibration curve intercept and slope values, along with standard errors

	Coefficients	*Standard Error*	*Lower 95%*	*Upper 95%*
Intercept	0.83	0.98	-1.30	2.96
Slope	6.53	0.31	5.86	7.21

With 95% confidence, the intercept is between -1.3 to 2.96 mA/cm^2, and the slope is between 5.86 to 7.21 mA/cm^2/log$_{10}$(Conc(pM)).

The lower and upper limits of the intercept and slope values were employed to calculate four possible extreme values of LOD, using the modified LOD formula,

$$\mathrm{LOD} = \frac{3.3\times \text{ stdev - intercept}}{\text{slope}}$$

The resulting values of LODs are 4, 5, 15 and 29 pM. i.e., The corresponding 95% confidence interval for LOD is 4 - 29 pM. The nominal LOD value based on an intercept of 0.83 and slope of 6.53 is 10 pM.

S14. Summary of literature reports on CHIKV detection

Table S14. Summary of literature reports on detection of CHIKV, along with LOD and linear range.

#	Method	Target	Substrate	LOD	Linear Range	Reference
1	Optical, surface plasmon resonance (SPR)	Infected plasma/ platelets	Graphene /Si/Ag layers on glass prism	-	-	[8]
2	Optical (SPR)	Infected plasma/ platelets	$PtSe_2$/Si/Ag on BK7 prism	-	-	[9]
3	Piezoelectric sensing	CHIKV antibody	SiO_2 (MEMS Cantilever)	-	-	[10]
4	Electrochemical (EIS)	CHIKV	Cysteine/ZnONP/ Concanavalin A	1:50 dilution	-	[11]
5	Electrochemical (CV)	CHIKV	Zn-Ag nanocomposite	1 ng/mL	1 ng/mL – 100 µg/mL	[12]
6	Electrochemical (EIS)	CHIKV	Au–polyaniline and sulfur, N_2-doped graphene quantum dot nanocomposites	22.1 fg/mL	100 fg/mL – 1 ng/mL	[13]
7	Electrochemical (CV, DPV)	CHIKV target DNA	Au shell coated magnetic nanocubes	0.1 nM (4 ng/mL)	0.1 nM– 100 µM	[14]
8	Electrochemical (CV)	CHIKV	AgNP based carbon ink	0.1 ng/mL	0.1 ng/mL– 1 µg/mL	[15]
9	Electrochemical (CV)	CHIKV	Nano graphone oxide/ZnO	1 ng/mL	1 ng/mL – 10 µg/mL	[16]
10	Electrochemical (SWV)	CHIKV E1	Au PCB	10 pM (0.4 ng/mL)	5 pM -100 nM (0.2 ng/mL – 4 µg/mL)	Present work

S15. Repeatability and Reproducibility

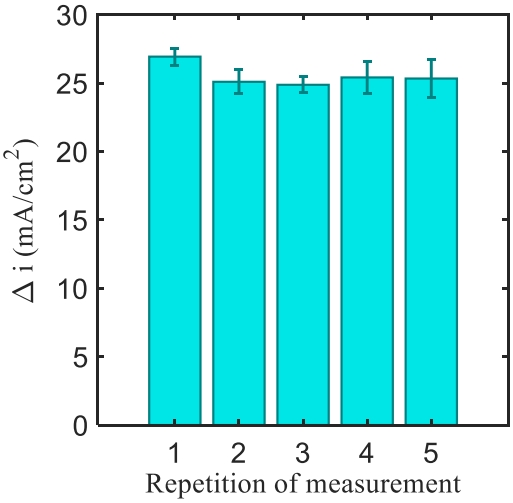

Figure S15.1. The change in SWV current for sensing CHIKV E1 (10 nM) using five different aptasensors

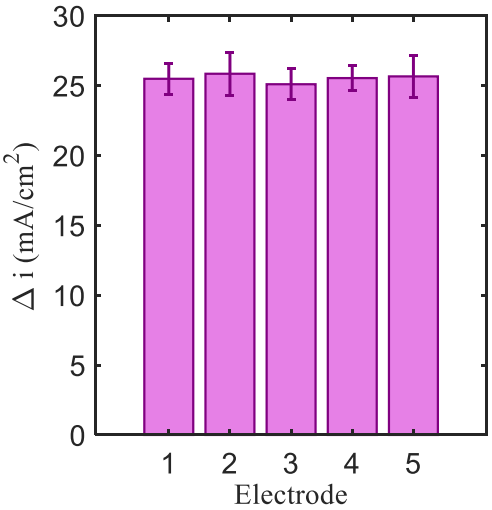

Figure S15.2. The results of five repetitive measurements - change in SWV current for sensing CHIKV E1 (10 nM) on the aptasensor

S16.Stability at room temperature

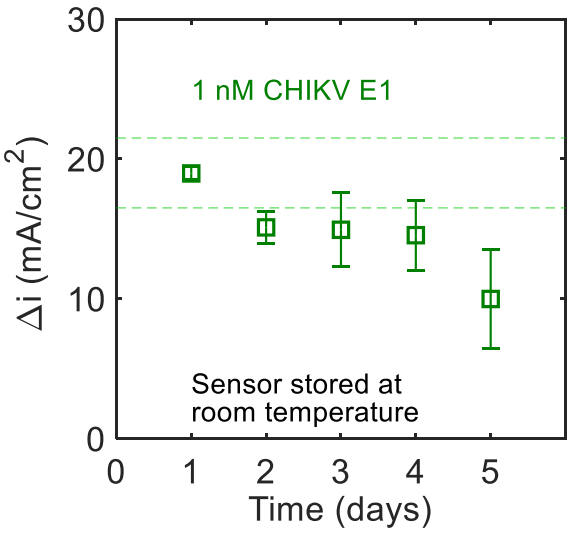

Figure S16. Stability and producibility of the sensor stored at room temperature.

Figure S16 shows that when the sensor is stored at room temperature (~ 27 °C), its performance degrades quickly. In comparison, when the sensor is stored at 4 °C, its performance is good for 10 days (Fig. 9B). Hence it is recommended to store the sensor at 4 °C.

References

1. Q. Yang, J. Pedreira-Rincón, L. Balerdi-Sarasola, L. Baptista-Pires, J. Muñoz, D. Camprubí-Ferrer, A. Idili and C. Parolo, *Biosens. Bioelectron.*, 2025, **274**, 117152.

2. G.-C. Zhao and X. Yang, *Electrochem. Commun.*, 2010, **12**, 300-302.

3. A. Shaver, S. D. Curtis and N. Arroyo-Curras, *ACS applied materials & interfaces*, 2020, **12**, 11214-11223.

4. L. M. Fischer, M. Tenje, A. R. Heiskanen, N. Masuda, J. Castillo, A. Bentien, J. Émneus, M. H. Jakobsen and A. Boisen, *Microelectron. Eng.*, 2009, **86**, 1282-1285.

5. R. Nandeshwar, M. S. Kumar, K. Kondabagil and S. Tallur, *IEEE Access*, 2021, **9**, 154368-154377.

6. R. Agarwal, *ACS Electrochemistry*, 2025.

7. C.-Y. Lai, W.-C. Huang, J.-H. Weng, L.-C. Chen, C.-F. Chou and P.-K. Wei, *Electrochim. Acta*, 2020, **337**, 135750.

8. P. Yupapin, Y. Trabelsi, D. Vigneswaran, S. A. Taya, M. G. Daher and I. Colak, *Plasmonics*, 2022, **17**, 1315-1321.

9. T. I. Singh, P. Singh and B. Karki, *Plasmonics*, 2023, **18**, 1173-1180.

10. M. Katta and R. Sandanalakshmi, *Sens. Bio-Sens. Res.*, 2021, **32**, 100413.

11. E. P. Simão, D. B. Silva, M. T. Cordeiro, L. H. Gil, C. A. Andrade and M. D. Oliveira, *Talanta*, 2020, **208**, 120338.

12. P. Sharma, H. Hassan, M. R. Hasan, T. Fatima, H. Mohan, M. Khanuja, S. Kaushik and J. Narang, *Biosens. Bioelectron. X*, 2023, **13**, 100303.

13. F. Nasrin, K. Tsuruga, D. I. S. Utomo, A. D. Chowdhury and E. Y. Park, *Biosensors*, 2021, **11**, 376.

14. C. Singhal, A. Dubey, A. Mathur, C. Pundir and J. Narang, *Process Biochem.*, 2018, **74**, 35-42.

15. P. Sharma, M. R. Hasan, U. M. Naikoo, S. Khatoon, R. Pilloton and J. Narang, *Biosensors*, 2024, **14**, 344.

16. P. Sharma, M. R. Hasan, M. Khanuja and J. Narang, *Microchem. J.*, 2025, **212**, 113474.